

Gapless Dirac surface states in the antiferromagnetic topological insulator MnBi_2Te_4

Przemyslaw Swatek,^{1,2} Yun Wu,^{1,2} Lin-Lin Wang,¹ Kyungchan Lee,^{1,2}
Benjamin Schruink,^{1,2} Jiaqiang Yan,^{3,4,*} and Adam Kaminski^{1,2,†}

¹*Division of Materials Science and Engineering, Ames Laboratory, Ames, Iowa 50011, USA*

²*Department of Physics and Astronomy, Iowa State University, Ames, Iowa 50011, USA*

³*Materials Science and Technology Division, Oak Ridge National Laboratory, Oak Ridge, Tennessee 37831, USA*

⁴*Department of Materials Science and Engineering,*

University of Tennessee, Knoxville, Tennessee 37996, USA

(Dated: February 19, 2024)

We use high-resolution, tunable angle-resolved photoemission spectroscopy (ARPES) and density functional theory (DFT) calculations to study the electronic properties of single crystals of MnBi_2Te_4 , a material that was predicted to be the first intrinsic antiferromagnetic (AFM) topological insulator. We observe both bulk and surface bands in the electronic spectra, in reasonable agreement with the DFT calculations results. In striking contrast to the earlier literatures showing a full gap opening between two surface band manifolds along (0001) direction, we observed a gapless Dirac cone remain protected in MnBi_2Te_4 across the AFM transition ($T_N = 24$ K). Our data also reveal the existence of a second Dirac cone closer to the Fermi level, predicted by band structure calculations. Whereas the surface Dirac cones seem to be remarkably insensitive to the AFM ordering, we do observe splitting of the bulk band that develops below the T_N . Having a moderately high ordering temperature, MnBi_2Te_4 provides a unique platform for studying the interplay between topology and magnetic ordering.

The discovery of different types of exotic topological states that can be experimentally realized in semimetals has ignited intensive studies [1–7]. Besides their unprecedented importance for fundamental science, they also offer intriguing possibilities for device design revolutionizing computation capabilities, as well as laser technology [8]. Among them, magnetic topological semimetals and insulators are promising materials for spintronics, especially in the context of the new generation of logic or memory devices. [9–13] The key challenge is to find new materials that provide desired spin structure at the chemical potential and allow an easy way for spin manipulation.

Antiferromagnetic topological insulators (AFM-TI) constitute a new unique subclass of topological quantum materials with additional magnetic degrees of freedom [14, 15]. They have a bulk band gap, but at the same time their surface states can be protected by $S = \Theta T_{1/2}$ symmetry, defined as the product of the time-reversal symmetry (TRS) Θ and the nonsymmorphic translation $T_{1/2}$. The preservation of S symmetry provides surface states a protection from backscattering by non-trivial Z_2 topology even if the TRS is broken. Such remarkable properties of these materials open new opportunities, for example, for investigating the magnetoelectric effect. [2] To observe such phenomenon, it is necessary to gap out the Dirac cone by breaking the $T_{1/2}$ symmetry in intrinsic AFM-TIs by choosing a specific surface orientation [14, 16]. However, despite tremendous theoretical and experimental efforts to find new AFM-TIs in single crystalline form [17–20], obtaining good quality AFM-TI material is very challenging.

Very recently, one of the magnetic variants of well-

studied Bi_2Te_3 family 3D TIs [21, 22] - MnBi_2Te_4 - has been theoretically proposed to be the first intrinsically stoichiometric AFM-TI, where the novel Z_2 topological invariant was protected by the S symmetry in the A-type AFM configuration [17, 18, 23–30]. Its unusual electronic structure opens a route to study different variants of topological phenomena including 2D and 3D magnetic interaction, quantum anomalous Hall effect (QAH), axion states, chiral Majorana modes and an elusive single pair of Weyl nodes near the Fermi level [31–34]. Such peculiar properties of the electronic states can be realized in MnBi_2Te_4 by breaking the S symmetry on the (0001) surface due to magnetic phase transition. [23] Its magnetic moments along c axis are produced by the manganese sub-lattice with $C3v$ symmetry. In turn, its non-trivial topological surface states are formed by band inversion between $\text{Bi-}p_z^+$ and $\text{Te-}p_z^-$ states with $C3v$ and $D3d$ group symmetry due to SOC, and in consequence drives the system to a Chern insulator phase. [23, 29] Because MnBi_2Te_4 is built of the stacking blocks of Te-Bi-Te-Mn-Te-Bi-Te septuple layers composed of single atomic sheets, breaking the S symmetry can be achieved by cleavage sample surface along (0001) direction or by adjusting the magnetic degree of freedom and inducing a transition from AFM to FM state by magnetic field. The magnetic structure with A-type AFM order is required for the occurrence of the gap in the 2D surface Dirac cone [18, 23] and has been recently determined by neutron diffraction in the bulk. [35]

Here, we present high-resolution ARPES data and first-principles calculations to investigate the surface states and bulk properties of MnBi_2Te_4 . Since MnBi_2Te_4 has a relatively high Neel temperature $T_N = 24$ K, we

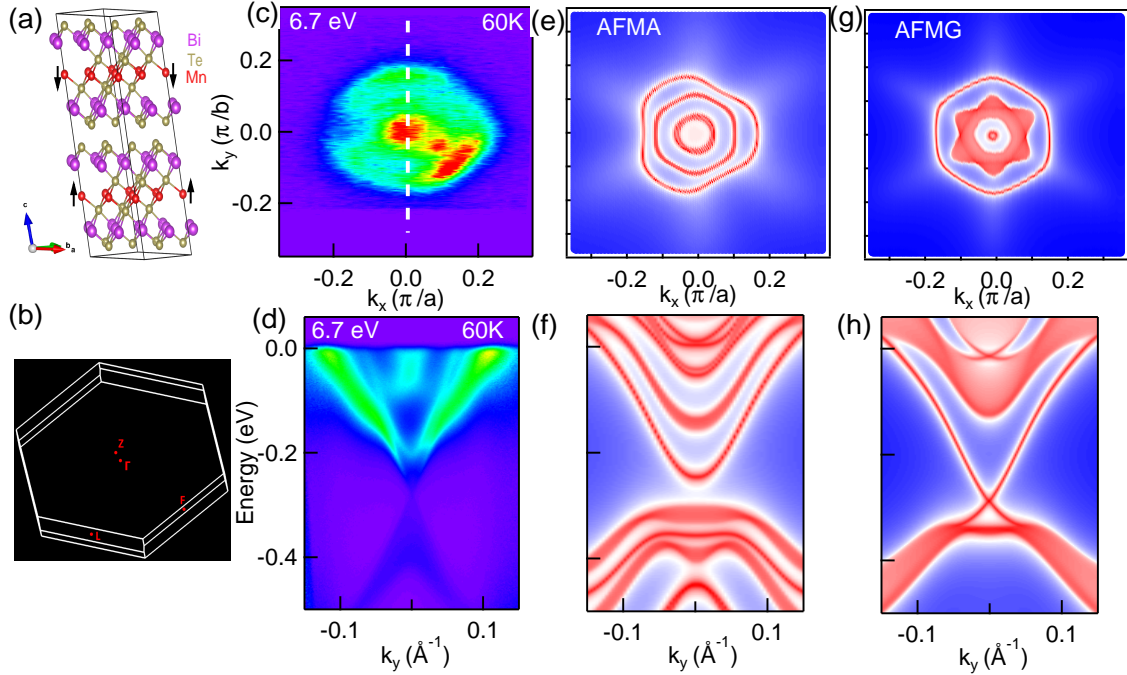


FIG. 1. Crystal and electronic structure of MnBi_2Te_4 . (a) Crystal structure of MnBi_2Te_4 (Mn, red spheres; Bi, purple spheres; Te, gold spheres) with A-type AFM (AFMA) configurations. Doubling the periodicity with in-plane AFM gives an AFMG structure. (b) Brillouin zone of MnBi_2Te_4 . (c) Fermi surface plot - ARPES intensity integrated within 10 meV about the chemical potential measured using 6.7 eV photons at 60 K. (d) Band dispersion along the high symmetry line as shown in (c). (e) Calculated Fermi surface of MnBi_2Te_4 with AFMA configuration using a semi-infinite (0001) surface. (f) Calculated electronic structure of MnBi_2Te_4 with AFMA configuration along the white dashed line in (c). (g) Calculated Fermi surface of MnBi_2Te_4 with G-type AFM configuration using a semi-infinite (0001) surface. (h) Calculated electronic structure of MnBi_2Te_4 with AFMG configuration along the white dashed line in (c).

collected our ARPES data at 60 K and 8 K, e.g. far above and below AFM ordering. Unlike early ARPES findings of a surface state band gap ranging from about 50 meV to 200 meVs centered at binding energy of 300 meV at the Γ point, [26, 27, 30, 34] we did not find any evidence for an opening of a gap at the Dirac point of the topological surface states. Furthermore, we do not see any difference in the spectral region around the Dirac point between paramagnetic and antiferromagnetic states. Also, we identified another 2D Dirac point with a binding energy of 50 meV on the same (0001) surface, originating from a nontrivial Z_2 topology. All of our experimental findings are supported by the band calculations based on a DFT calculation including SOC and assuming AFMG magnetic moment alignment. Finally, we also reveal the effect of AFM ordering on the electronic band structure in MnBi_2Te_4 . Our findings provide a great platform for discovering new unusual quantum phases emerging due to the interplay of different types of magnetism with the topological states in one single crystal.

Single crystals of MnBi_2Te_4 were grown out of a Bi-Te flux [35]. Platelike samples used for ARPES measurements were cleaved *in situ* at 60 K under ultra-high vacuum (UHV). The data were acquired using a

tunable VUV laser ARPES system, that consists of a Omicron Scienta DA30 electron analyzer, a picosecond Ti:Sapphire oscillator and fourth harmonic generator [36]. Data were collected with photon energies of 6.7 and 6.36 eV. Momentum and energy resolutions were set at $\sim 0.005 \text{ \AA}^{-1}$ and 2 meV. The size of the photon beam on the sample was $\sim 30 \text{ }\mu\text{m}$.

Band structures with spin-orbit coupling (SOC) in density functional theory (DFT) [37, 38] have been calculated using a PBE [39] exchange-correlation functional, a plane-wave basis set and projector augmented wave method [40] as implemented in VASP [41, 42]. To account for the half-filled strongly localized Mn 3d orbitals, a Hubbard-like U [43] value of 3.0 eV is used. For bulk band structure of A-type anti-ferromagnetic (AFMA) MnBi_2Te_4 , the rhombohedral unit cell is doubled along c direction with a Monkhorst-Pack [44] $(9 \times 9 \times 3)$ k -point mesh including the Γ point and a kinetic energy cutoff of 270 eV. The band structure of the G-type anti-ferromagnetic (AFMG) configuration is calculated by further doubling the rhombohedral unit cell in the other two directions. Experimental lattice parameters [45] have been used with atoms fixed in their bulk positions. A tight-binding model based on maximally lo-

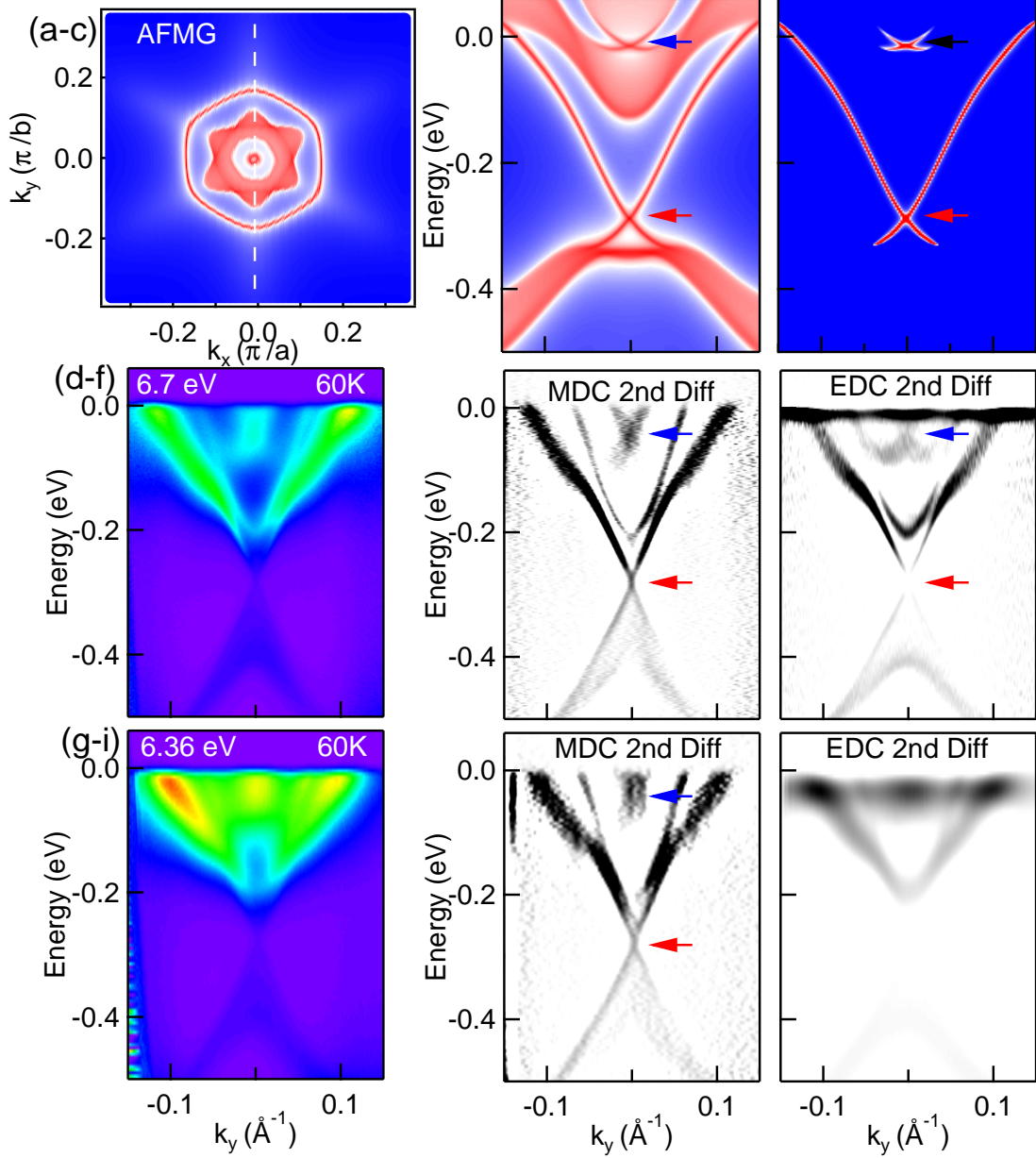


FIG. 2. Fermi surface plot and band dispersions of MnBi₂Te₄. (a) Calculated Fermi surface of MnBi₂Te₄ with G-type AFM configuration using a semi-infinite (001) surface. (b) Calculated electronic structure of MnBi₂Te₄ along the white dashed line in (a). (c) Surface states extracted from (b). (d) Band dispersion along the white dashed line in (a) measured using 6.7 eV photons at 60 K. (e-f) Second derivatives of ARPES intensity map in panel (d) with respect to MDC and EDC, respectively. (g) Band dispersion along the white dashed line in (a) measured using 6.36 eV photons at 60 K. (h-i) Second derivatives of ARPES intensity map in panel (g) with respect to MDC and EDC, respectively. The blue [black in (c)] and red arrows in panels (c), (e), (f), (h) point to the first and second Dirac point at two binding energies, respectively.

calized Wannier functions [46–48] was constructed to reproduce closely the bulk band structure including SOC in the range of $E_F \pm 1$ eV with Mn *sd*, Bi *p* and Te *p* orbitals. Then the spectral functions and Fermi surface of a semi-infinite MnBi₂Te₄ (001) surface were calculated with the surface Greens function methods [49–52] as implemented in WannierTools [53].

Figures 1(a) shows the crystal structure and A-type AFM (AFMA) magnetic orderings of MnBi₂Te₄. G-type AFM (AFMG) configuration can be generated by further doubling the rhombohedral unit cell in the other two directions. In the AFMA configuration, the *S* symmetry is broken on the (0001) surface. However, in the AFMG configuration, breaking only the one along *c* axis

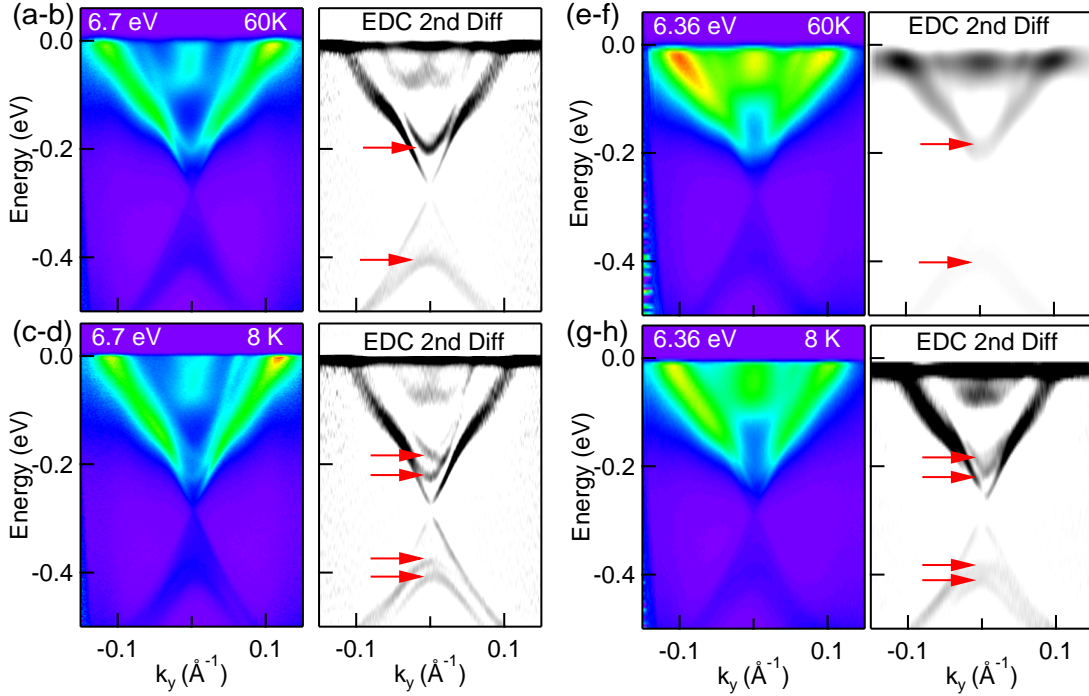


FIG. 3. Temperature evolution of the band dispersions measured using 6.7 and 6.36 eV. (a) Band dispersion along the white dashed line in Fig. 2(a) measured using 6.7 eV photons at 60 K. (b) Second derivative of ARPES intensity map in panel (a) with respect to EDC. (c-d) Similar to (a-b) but measured at 8 K. (e) Band dispersion along the white dashed line in Fig. 2(a) measured using 6.36 eV photons at 60 K. (f) Second derivative of ARPES intensity map in panel (a) with respect to EDC. (g-h) Similar to (e-f) but measured at 8 K. Red arrows in panels (d) and (h) point to the splitting of the bulk bands under magnetic transition.

on (0001) surface does not gap out DP, because the two others along a and b axis still remain. Thus, we would expect to observe gapless topological surface states on this surface. Fig. 1(c) shows the ARPES intensity plots of MnBi_2Te_4 measured using 6.7 eV photons at 60 K. Two shallow electron pockets and a blob of intensity can be seen at the Γ point. Fig. 1(d) shows the band dispersion along the white dashed line in panel (c), where two large and one shallow electron pocket can be easily identified. Surprisingly, a gapless Dirac state is clearly present, in stark contrast to the previous predictions and ARPES results [17, 18, 23–30]. To elucidate the origin of this gapless Dirac state, we conducted DFT calculations on two types of magnetic moment configurations: A-type AFM and G-type AFM. In Figs. 1(e) and (f), we can see that the Fermi surface and band dispersion from DFT calculations partially agree with the ARPES results, whereas the significant gapless Dirac state is missing. On the other hand, with the AFMG configuration, the Fermi surface and band dispersion from DFT calculations reproduce the ARPES intensity pretty well. In order to achieve a better match between DFT and ARPES results, we have to shift the chemical potential of DFT calculations upwards by roughly 220 meV, which is probably due to the lattice defects [35].

In Fig. 2, we presented the DFT calculations and ARPES intensities of MnBi_2Te_4 in great detail. Fig. 2(c) shows the surface state contribution extracted from the DFT calculation results shown in panel (b). Other than the Dirac point marked by the red arrow, we can also identify another Dirac point marked by the blue arrow in panels (b) and (c). These surface Dirac states are protected by the effective TRS in the AFMG configuration, which has yet to be accounted for. To demonstrate that these two Dirac surface states indeed exist in the ARPES spectra, we plotted the second derivative of ARPES intensity with respect to momentum distribution curve (MDC) and energy distribution curve (EDC) in panels (e) and (f). We can clearly see that there are two distinct Dirac points at the binding energies of 50 and 280 meV as marked by the blue and red arrows, respectively. Similar features can be identified in the ARPES intensity measured using 6.36 eV photons at 60 K, as shown in panel (h). These results clearly demonstrate that there are two instead of just one gapless Dirac surface states on the (0001) surface in MnBi_2Te_4 .

Next, let's focus on the temperature evolution of the electronic structure in MnBi_2Te_4 as shown in Fig. 3. Panel (b) shows the second derivative of the ARPES intensity calculated with respect to EDC measured using

6.7 eV at 60 K (above the $T_N = 24$ K). Other than the two gapless Dirac surface states identified in Fig. 2, we can also observe parabolic conduction and valence bands marked by the red arrows as shown in panel (b). Upon cooling the sample temperature down to 8 K [panels (c)-(d)], we can see that the single conduction band splits into two bands as marked by the two red arrows close to binding energy of 200 meV in panel (d). The same happened to the valence band sitting at $E_B=400$ meV measured using both 6.7 and 6.36 eV photons as shown in panels (d) and (h), respectively. Since MnBi_2Te_4 undergoes an AFM instead of FM transition, this splitting of the band is probably due to the bulk-surface interlayer ferromagnetic coupling. On the other hand, the two gapless Dirac surface states does not seem to be correlated with the bulk AFM transition, implicating that the surface may have a different configuration (i.e. AFMG) from the bulk (i.e. AFMA) [54].

In conclusion, we presented high-resolution ARPES data and first-principles calculations to investigate the electronic properties of MnBi_2Te_4 . In contrast to the observation of gapped surface state at the Γ point from early ARPES measurements [26, 27, 30, 34], we observed two gapless topological surface states with Dirac points sitting at roughly 50 and 280 meV below Fermi level. Furthermore, the gapless Dirac state does not evolve along with the magnetic transition. On the contrary, the bulk states showed a significant band splitting below the transition, which is probably due to the interlayer ferromagnetic exchange correlation with the surface. Further studies of surface magnetism are required in order to validate this scenario.

Upon completion of this project we become aware that other groups [55–57] also independently studied MnBi_2Te_4 and showed an indication of a single gapless surface Dirac cone in this compound.

Research at Ames Laboratory and ORNL was supported by the U.S. Department of Energy, Office of Basic Energy Sciences, Division of Materials Science and Engineering. P. S and Y. W were supported by the Center for the Advancement of Topological Semimetals, an Energy Frontier Research Center funded by the U.S. DOE, Office of Basic Energy Sciences. Ames Laboratory is operated for the U.S. Department of Energy by Iowa State University under Contract No. DE-AC02-07CH11358. B. S. was supported by CEM, a NSF MRSEC, under Grant No. DMR-1420451.

Data for figures are available at <https://doi.org/>.

* yanj@ornl.gov

† kaminski@ameslab.gov

[1] M. Z. Hasan and C. L. Kane, *Rev. Mod. Phys.* **82**, 3045 (2010).

- [2] Y. Tokura, K. Yasuda, and A. Tsukazaki, *Nature Reviews Physics* **1**, 126 (2019).
- [3] D. Hsieh, D. Qian, L. Wray, Y. Xia, Y. S. Hor, R. J. Cava, and M. Z. Hasan, *Nature* **452**, 970 (2008).
- [4] E. Gibney, *Nature* **560**, 151 (2018).
- [5] C.-K. Chiu, J. C. Y. Teo, A. P. Schnyder, and S. Ryu, *Rev. Mod. Phys.* **88**, 035005 (2016).
- [6] L. Plucinski, *Journal of Physics: Condensed Matter* **31**, 183001 (2019).
- [7] L. M. Schoop, F. Pielnhofer, and B. V. Lotsch, *Chemistry of Materials* **30**, 3155 (2018).
- [8] M. A. Bandres, S. Wittek, G. Harari, M. Parto, J. Ren, M. Segev, D. N. Christodoulides, and M. Khajavikhan, *Science* **359**, eaar4005 (2018).
- [9] S. Manipatruni, D. E. Nikonov, C.-C. Lin, T. A. Gosavi, H. Liu, B. Prasad, Y.-L. Huang, E. Bonturim, R. Ramesh, and I. A. Young, *Nature* **565**, 35 (2018).
- [10] L. Šmejkal, Y. Mokrousov, B. Yan, and A. H. MacDonald, *Nature Physics* **14**, 242 (2018).
- [11] D. Pesin and A. H. MacDonald, *Nature Materials* **11**, 409 (2012).
- [12] M. Jamali, J. S. Lee, J. S. Jeong, F. Mahfouzi, Y. Lv, Z. Zhao, B. K. Nikolić, K. A. Mkhoyan, N. Samarth, and J.-P. Wang, *Nano Letters* **15**, 7126 (2015).
- [13] M. G. Mankalale, Z. Zhao, J.-P. Wang, and S. S. Sapatnekar, *IEEE Transactions on Electron Devices* **66**, 1990 (2019).
- [14] R. S. K. Mong, A. M. Essin, and J. E. Moore, *Phys. Rev. B* **81**, 245209 (2010).
- [15] J. E. Moore, *Nature (London)* **464**, 194 (2010).
- [16] A. M. Essin, J. E. Moore, and D. Vanderbilt, *Phys. Rev. Lett.* **102**, 146805 (2009).
- [17] J. Li, Y. Li, S. Du, Z. Wang, B.-L. Gu, S.-C. Zhang, K. He, W. Duan, and Y. Xu, *Science Advances* **5**, eaaw5685 (2019).
- [18] S. Chowdhury, K. F. Garrity, and F. Tavazza, *npj Computational Materials* **5** (2019), 10.1038/s41524-019-0168-1.
- [19] Y. Xu, Z. Song, Z. Wang, H. Weng, and X. Dai, *Physical Review Letters* **122** (2019), 10.1103/physrevlett.122.256402.
- [20] L.-L. Wang, N. H. Jo, B. Kuthanazhi, Y. Wu, R. J. McQueeney, A. Kaminski, and P. C. Canfield, *Phys. Rev. B* **99**, 245147 (2019).
- [21] Y. L. Chen, J. G. Analytis, J.-H. Chu, Z. K. Liu, S.-K. Mo, X. L. Qi, H. J. Zhang, D. H. Lu, X. Dai, Z. Fang, S. C. Zhang, I. R. Fisher, Z. Hussain, and Z.-X. Shen, *Science* **325**, 178 (2009).
- [22] R. Jiang, L.-L. Wang, M. Huang, R. S. Dhaka, D. D. Johnson, T. A. Lograsso, and A. Kaminski, *Phys. Rev. B* **86**, 085112 (2012).
- [23] M. M. Otrokov, I. I. Klimovskikh, H. Bentmann, A. Zeugner, Z. S. Aliev, S. Gass, A. U. B. Wolter, A. V. Koroleva, D. Estyunin, A. M. Shikin, M. Blanco-Rey, M. Hoffmann, A. Y. Vyazovskaya, S. V. Ereemeev, Y. M. Koroteev, I. R. Amiraslanov, M. B. Babanly, N. T. Mamedov, N. A. Abdullayev, V. N. Zverev, B. Behner, E. F. Schwier, S. Kumar, A. Kimura, L. Petaccia, G. D. Santo, R. C. Vidal, S. Schatz, K. Kiner, C.-H. Min, S. K. Moser, T. R. F. Peixoto, F. Reinert, A. Ernst, P. M. Echenique, A. Isaeva, and E. V. Chulkov, *arXiv:1809.07389* (2018).
- [24] Y. Gong, J. Guo, J. Li, K. Zhu, M. Liao, X. Liu, Q. Zhang, L. Gu, L. Tang, X. Feng, D. Zhang, W. Li,

- C. Song, L. Wang, P. Yu, X. Chen, Y. Wang, H. Yao, W. Duan, Y. Xu, S.-C. Zhang, X. Ma, Q.-K. Xue, and K. He, *Chinese Physics Letters* **36**, 076801 (2019).
- [25] M. M. Otrokov, I. P. Rusinov, M. Blanco-Rey, M. Hoffmann, A. Y. Vyazovskaya, S. V. Ereemeev, A. Ernst, P. M. Echenique, A. Arnau, and E. V. Chulkov, *Phys. Rev. Lett.* **122**, 107202 (2019).
- [26] A. Zeugner, F. Nietschke, A. U. B. Wolter, S. Gaß, R. C. Vidal, T. R. F. Peixoto, D. Pohl, C. Damm, A. Lubk, R. Hentrich, S. K. Moser, C. Fornari, C. H. Min, S. Schatz, K. Kißner, M. Ünzelmann, M. Kaiser, F. Scaravaggi, B. Rellinghaus, K. Nielsch, C. Hess, B. Büchner, F. Reinert, H. Bentmann, O. Oeckler, T. Doert, M. Ruck, and A. Isaeva, *Chemistry of Materials* **31**, 2795 (2019).
- [27] R. C. Vidal, H. Bentmann, T. R. F. Peixoto, A. Zeugner, S. Moser, C. H. Min, S. Schatz, K. Kissner, M. Ünzelmann, C. I. Fornari, H. B. Vasili, M. Valvidares, K. Sakamoto, J. Fujii, I. Vobornik, T. K. Kim, R. J. Koch, C. Jozwiak, A. Bostwick, J. D. Denlinger, E. Rotenberg, J. Buck, M. Hoesch, F. Diekmann, S. Rohlf, M. Kallne, K. Rossnagel, M. M. Otrokov, E. V. Chulkov, M. Ruck, A. Isaeva, and F. Reinert, *arXiv:1903.11826* (2019).
- [28] J. Q. Yan, S. Okamoto, M. A. McGuire, A. F. May, R. J. McQueeney, and B. C. Sales, *arXiv:1905.00400* (2019).
- [29] J. Li, C. Wang, Z. Zhang, B.-L. Gu, W. Duan, and Y. Xu, *arXiv:1905.00642* (2019).
- [30] B. Chen, F. Fei, D. Zhang, B. Zhang, W. Liu, S. Zhang, P. Wang, B. Wei, Y. Zhang, Z. Zuo, J. Guo, Q. Liu, Z. Wang, X. Wu, J. Zong, X. Xie, W. Chen, Z. Sun, D. Shen, S. Wang, Y. Zhang, M. Zhang, X. Wang, F. Song, H. Zhang, and B. Wang, *arXiv:1903.09934* (2019).
- [31] D. Zhang, M. Shi, T. Zhu, D. Xing, H. Zhang, and J. Wang, *Phys. Rev. Lett.* **122**, 206401 (2019).
- [32] C. Liu, Y. Wang, H. Li, Y. Wu, Y. Li, J. Li, K. He, Y. Xu, J. Zhang, and Y. Wang, *arXiv:1905.00715* (2019).
- [33] N. Varnava and D. Vanderbilt, *Phys. Rev. B* **98**, 245117 (2018).
- [34] S. H. Lee, Y. Zhu, Y. Wang, L. Miao, T. Pillsbury, S. Kempinger, D. Graf, N. Alem, C.-Z. Chang, N. Samarth, and Z. Mao, *arXiv:1812.00339* (2018).
- [35] J.-Q. Yan, Q. Zhang, T. Heitmann, Z. Huang, K. Y. Chen, J.-G. Cheng, W. Wu, D. Vaknin, B. C. Sales, and R. J. McQueeney, *Phys. Rev. Materials* **3**, 064202 (2019).
- [36] R. Jiang, D. Mou, Y. Wu, L. Huang, C. D. McMillen, J. Kolis, H. G. Giesber, J. J. Egan, and A. Kaminski, *Review of Scientific Instruments* **85**, 033902 (2014).
- [37] P. Hohenberg and W. Kohn, *Phys. Rev.* **136**, B864 (1964).
- [38] W. Kohn and L. J. Sham, *Phys. Rev.* **140**, A1133 (1965).
- [39] J. P. Perdew, K. Burke, and M. Ernzerhof, *Phys. Rev. Lett.* **77**, 3865 (1996).
- [40] P. E. Blöchl, *Phys. Rev. B* **50**, 17953 (1994).
- [41] G. Kresse and J. Furthmüller, *Phys. Rev. B* **54**, 11169 (1996).
- [42] G. Kresse and J. Furthmüller, *Computational Materials Science* **6**, 15 (1996).
- [43] S. L. Dudarev, G. A. Botton, S. Y. Savrasov, C. J. Humphreys, and A. P. Sutton, *Phys. Rev. B* **57**, 1505 (1998).
- [44] H. J. Monkhorst and J. D. Pack, *Phys. Rev. B* **13**, 5188 (1976).
- [45] D. S. Lee, T.-H. Kim, C.-H. Park, C.-Y. Chung, Y. S. Lim, W.-S. Seo, and H.-H. Park, *CrystEngComm* **15**, 5532 (2013).
- [46] N. Marzari and D. Vanderbilt, *Phys. Rev. B* **56**, 12847 (1997).
- [47] I. Souza, N. Marzari, and D. Vanderbilt, *Phys. Rev. B* **65**, 035109 (2001).
- [48] N. Marzari, A. A. Mostofi, J. R. Yates, I. Souza, and D. Vanderbilt, *Rev. Mod. Phys.* **84**, 1419 (2012).
- [49] D. H. Lee and J. D. Joannopoulos, *Phys. Rev. B* **23**, 4988 (1981).
- [50] D. H. Lee and J. D. Joannopoulos, *Phys. Rev. B* **23**, 4997 (1981).
- [51] M. P. L. Sancho, J. M. L. Sancho, and J. Rubio, *Journal of Physics F: Metal Physics* **14**, 1205 (1984).
- [52] M. P. L. Sancho, J. M. L. Sancho, J. M. L. Sancho, and J. Rubio, *Journal of Physics F: Metal Physics* **15**, 851 (1985).
- [53] Q. Wu, S. Zhang, H.-F. Song, M. Troyer, and A. A. Soluyanov, *arXiv preprint arXiv:1703.07789* (2017).
- [54] D. Mou, A. Sapkota, H.-H. Kung, V. Krapivin, Y. Wu, A. Kreyssig, X. Zhou, A. I. Goldman, G. Blumberg, R. Flint, and A. Kaminski, *Phys. Rev. Lett.* **116**, 196401 (2016).
- [55] Y.-J. Hao, P. Liu, Y. Feng, X.-M. Ma, E. F. Schwier, M. Arita, S. Kumar, C. Hu, R. Lu, M. Zeng, *et al.*, *arXiv preprint arXiv:1907.03722* (2019).
- [56] Y. Chen, L. Xu, J. Li, Y. Li, C. Zhang, H. Li, Y. Wu, A. Liang, C. Chen, S. Jung, *et al.*, *arXiv preprint arXiv:1907.05119* (2019).
- [57] H. Li, S.-Y. Gao, S.-F. Duan, Y.-F. Xu, K.-J. Zhu, S.-J. Tian, W.-H. Fan, Z.-C. Rao, J.-R. Huang, J.-J. Li, Z.-T. Liu, W.-L. Liu, Y.-B. Huang, Y.-L. Li, Y. Liu, G.-B. Zhang, H.-C. Lei, Y.-G. Shi, W.-T. Zhang, H.-M. Weng, T. Qian, H. Ding, *et al.*, *arXiv preprint arXiv:1907.06491* (2019).